

Dielectric super-absorbing metasurfaces via PT symmetry breaking: supplement

JIANBO YU,¹ BINZE MA,¹ AO OUYANG,¹ PINTU GHOSH,¹  HAO LUO,¹  ARNAB PATTANAYAK,¹ SANDEEP KAUR,¹ MIN QIU,^{2,3} PAVEL BELOV,⁴  AND QIANG LI^{1,*} 

¹State Key Laboratory of Modern Optical Instrumentation, College of Optical Science and Engineering, Zhejiang University, Hangzhou 310024, China

²Key Laboratory of 3D Micro/Nano Fabrication and Characterization of Zhejiang Province, School of Engineering, Westlake University, Hangzhou 310024, China

³Institute of Advanced Technology, Westlake Institute for Advanced Study, Hangzhou 310024, China

⁴Department of Physics and Engineering, ITMO University, Russia

*Corresponding author: qiangli@zju.edu.cn

This supplement published with Optica Publishing Group on 1 October 2021 by The Authors under the terms of the [Creative Commons Attribution 4.0 License](https://creativecommons.org/licenses/by/4.0/) in the format provided by the authors and unedited. Further distribution of this work must maintain attribution to the author(s) and the published article's title, journal citation, and DOI.

Supplement DOI: <https://doi.org/10.6084/m9.figshare.16613329>

Parent Article DOI: <https://doi.org/10.1364/OPTICA.430893>

Dielectric super-absorbing metasurfaces via PT symmetry breaking: supplemental document

1. Super absorption with diabolic point degeneracies

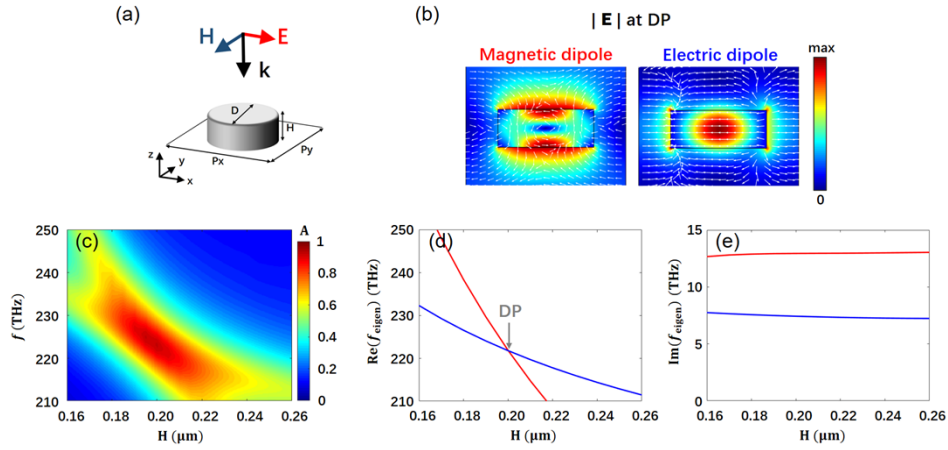


Fig. S1. **The system with diabolic point degeneracies.** (a) Schematic of the metasurface. (b) Eigenmodes of magnetic and electric dipole resonances at the DP. The color shows the electric field distribution at the plane of $y = 0$. The arrow shows the direction of electric field. (c) Absorption spectra at different disk's thickness H . (d) $\text{Re}(f_{\text{eigen}})$ and (e) $\text{Im}(f_{\text{eigen}})$ of the two modes at different disk's thickness H .

One typical two-orthogonal-mode system is shown in Fig. S1(a), which consists of periodic low-loss dielectric disks in uniform background. The orthogonality of magnetic and electric dipole modes supported by the metasurface makes the eigenfrequencies degenerate at the diabolic point (DP). At the DP, $\text{Re}(f_{\text{eigen}})$ of two modes are the same, whereas their associated eigenvectors are orthogonal. Therefore, two distinct eigenmodes can be found at the DP [Fig. S1(b)]. This condition is different from the EP degeneracies described in the main text [Fig. 2(c)]. The absorption spectra, $\text{Re}(f_{\text{eigen}})$ and $\text{Im}(f_{\text{eigen}})$ of the two modes at different disk's thickness H are calculated [Figs. S1(c)-S1(e)]. In the simulation, the refractive index of the cylinder is set to be $n = 4 + 0.1i$, other parameters are: $D = 0.480\mu\text{m}$, and $P_x = P_y = 0.800\mu\text{m}$.

2. Absorption of two modes with the same symmetric properties

For the photonic system plotted in the main text [Fig. 1(a)], when the mirror-plane symmetry about two ports is slightly disturbed (e.g. nanostructures with the low-index substrate and the air superstrate), we approximately suppose the resonant modes decay either symmetrically or anti-symmetrically into two ports, thus the two modes will have either the same or different symmetric properties. For each mode, we take $|\gamma_{je}| \approx |\gamma'_{je}|$. The relationship between input and output waves satisfies the following temporal coupled-mode equations [1]:

$$\frac{\partial \mathbf{A}}{\partial t} = -i\mathbf{H}\mathbf{A} + D^T \mathbf{S}_+ \quad (\text{S1})$$

$$\mathbf{S}_- = C\mathbf{S}_+ + D\mathbf{A} \quad (\text{S2})$$

where $\mathbf{A} = [A_1 \ A_2]^T$ is the resonance amplitude vector. $\mathbf{S}_+ = [S_{1+} \ 0]^T$ and $\mathbf{S}_- = [S_{1-} \ S_{2-}]^T$ represent the incoming and outgoing waves respectively. D is the 2×2 coupling matrix of the resonant modes with incoming or outgoing waves. C is the 2×2 scattering matrix of the incoming and outgoing waves in the absence of the resonant modes, with:

$$C = \begin{bmatrix} 0 & 1 \\ 1 & 0 \end{bmatrix} \quad (\text{S3})$$

Because of the energy conservation, we have

$$D^\dagger D = 2 \begin{bmatrix} \gamma_{1,R} & \beta \\ \beta^* & \gamma_{2,R} \end{bmatrix} \quad (\text{S4})$$

Therefore, the elements of matrix D are obtained as

$$|d_{11}| = |d_{21}| = \sqrt{\gamma_{1,R}} \quad (\text{S5})$$

$$|d_{12}| = |d_{22}| = \sqrt{\gamma_{2,R}} \quad (\text{S6})$$

where $d_{mn} = |d_{mn}|e^{-i(\theta_{mn})}$ ($m, n = 1, 2$), θ_{mn} is phase factor, and

$$\beta = \frac{1}{2} \sqrt{\gamma_{1,R}\gamma_{2,R}} [e^{-i(\theta_{12}-\theta_{11})} + e^{-i(\theta_{22}-\theta_{21})}] \quad (\text{S7})$$

When the two modes have the same symmetry properties (e.g. both M1 and M2 decay symmetrically, the anti-symmetrical condition is similar), we have $\theta_{11} = \theta_{21}$ and $\theta_{12} = \theta_{22}$. Therefore:

$$\beta = e^{-i(\theta_{12}-\theta_{11})} \sqrt{\gamma_{1,R}\gamma_{2,R}} \quad (\text{S8})$$

Based on time reversal, we have $CD^* = -D$, the coupled-mode equations can be expressed as

$$\frac{\partial}{\partial t} \begin{bmatrix} A_1 \\ A_2 \end{bmatrix} = \begin{bmatrix} -if_1 - \gamma_{1,NR} - \gamma_{1,R} & -i\kappa - \sqrt{\gamma_{1,R}\gamma_{2,R}} \\ -i\kappa - \sqrt{\gamma_{1,R}\gamma_{2,R}} & -if_2 - \gamma_{2,NR} - \gamma_{2,R} \end{bmatrix} \begin{bmatrix} A_1 \\ A_2 \end{bmatrix} + \begin{bmatrix} -i\sqrt{\gamma_{1,R}}S_{1+} \\ -i\sqrt{\gamma_{2,R}}S_{1+} \end{bmatrix} \quad (\text{S9})$$

$$\begin{bmatrix} S_{1-} \\ S_{2-} \end{bmatrix} = \begin{bmatrix} 0 \\ S_{1+} \end{bmatrix} + \begin{bmatrix} -i\sqrt{\gamma_{1,R}} & -i\sqrt{\gamma_{2,R}} \\ -i\sqrt{\gamma_{1,R}} & -i\sqrt{\gamma_{2,R}} \end{bmatrix} \begin{bmatrix} A_1 \\ A_2 \end{bmatrix} \quad (\text{S10})$$

When $f = f_1 = f_2$. The total absorption of the system is given by

$$A = \frac{2(\kappa^2 + \gamma_{1,NR}\gamma_{2,NR})(\gamma_{1,R}\gamma_{2,NR} + \gamma_{2,R}\gamma_{1,NR})}{[(\kappa^2 + \gamma_{1,NR}\gamma_{2,NR}) + (\gamma_{1,R}\gamma_{2,NR} + \gamma_{2,R}\gamma_{1,NR})]^2 + 4\kappa^2\gamma_{1,R}\gamma_{2,R}} \quad (\text{S11})$$

We finally have the absorption limit

$$A < \frac{2(\kappa^2 + \gamma_{1,NR}\gamma_{2,NR})(\gamma_{1,R}\gamma_{2,NR} + \gamma_{2,R}\gamma_{1,NR})}{[(\kappa^2 + \gamma_{1,NR}\gamma_{2,NR}) + (\gamma_{1,R}\gamma_{2,NR} + \gamma_{2,R}\gamma_{1,NR})]^2} \leq 0.5 \quad (\text{S12})$$

Therefore, when the two resonances have the same symmetry properties, the maximum absorption cannot exceed 50%.

3. Absorption of two modes with different symmetric properties

When the two modes have different symmetric properties, e.g. M1 decays symmetrically while M2 decays anti-symmetrically, we have $\theta_{11} = \theta_{21}$ and $\theta_{12} = \theta_{22} + \pi$. Based on time-reversal symmetry, we have $CD^* = -D$. Therefore, $\theta_{11} = \theta_{21} = \pi/2$, $\theta_{12} = \pi$, and $\theta_{22} = 0$. The far-field coupling coefficient is

$$\beta = -i(\sqrt{\gamma_{1e}\gamma_{2e}} - \sqrt{\gamma'_{1e}\gamma'_{2e}}) \quad (S13)$$

Since we have neglected the difference between $|\gamma_{je}|$ and $|\gamma'_{je}|$ due to the low index of substrate, we have $\beta \approx 0$. Two modes exchange energy with each other mainly through the near-field coupling, and the coupled-mode equations are given by

$$\frac{\partial}{\partial t} \begin{bmatrix} A_1 \\ A_2 \end{bmatrix} = \begin{bmatrix} -if_1 - \gamma_{1,NR} - \gamma_{1,R} & -i\kappa \\ -i\kappa & -if_2 - \gamma_{2,NR} - \gamma_{2,R} \end{bmatrix} \begin{bmatrix} A_1 \\ A_2 \end{bmatrix} + \begin{bmatrix} -i\sqrt{\gamma_{1,R}S_{1+}} \\ -i\sqrt{\gamma_{2,R}S_{1+}} \end{bmatrix} \quad (S14)$$

$$\begin{bmatrix} S_{1-} \\ S_{2-} \end{bmatrix} = \begin{bmatrix} 0 \\ S_{1+} \end{bmatrix} + \begin{bmatrix} -i\sqrt{\gamma_{1,R}} & -\sqrt{\gamma_{2,R}} \\ -i\sqrt{\gamma_{1,R}} & \sqrt{\gamma_{2,R}} \end{bmatrix} \begin{bmatrix} A_1 \\ A_2 \end{bmatrix} \quad (S15)$$

In the PT symmetry breaking regime, $f_1 = f_2$. At the resonant frequencies where $f = f_1 = f_2$, the reflection and transmission coefficients are given by

$$r = \frac{-2\kappa\sqrt{\gamma_{1,R}\gamma_{2,R}} + \gamma_{1,R}\gamma_{2,NR} - \gamma_{2,R}\gamma_{1,NR}}{-\kappa^2 - [\gamma_{1,R} + \gamma_{1,NR}][\gamma_{2,R} + \gamma_{2,NR}]} \quad (S16)$$

$$t = \frac{-\kappa^2 + \gamma_{1,R}\gamma_{2,R} - \gamma_{1,NR}\gamma_{2,NR}}{-\kappa^2 - [\gamma_{1,R} + \gamma_{1,NR}][\gamma_{2,R} + \gamma_{2,NR}]} \quad (S17)$$

Perfect absorption requires $r = t = 0$, therefore both Eq. (S22) and Eq. (S23) should be satisfied.

$$\gamma_{1,R}\gamma_{2,NR} - \gamma_{2,R}\gamma_{1,NR} = 2\kappa\sqrt{\gamma_{1,R}\gamma_{2,R}} \quad (S18)$$

$$\gamma_{1,R}\gamma_{2,R} - \gamma_{1,NR}\gamma_{2,NR} = \kappa^2 \quad (S19)$$

Eq. (S22) and Eq. (S23) can be re-expressed as

$$\frac{\gamma_{1,NR}}{\gamma_{1,R}} = 1 - \frac{\kappa}{\sqrt{\gamma_{1,R}\gamma_{2,R}}} \quad (S20)$$

$$\frac{\gamma_{2,NR}}{\gamma_{2,R}} = 1 + \frac{\kappa}{\sqrt{\gamma_{1,R}\gamma_{2,R}}} \quad (S21)$$

This is the perfect absorption condition [Eq. (3) and Eq. (4)] mentioned in the main text. The other condition: M1 decays anti-symmetrically and M2 decays symmetrically. We have $\theta_{12} = \theta_{22}$, and $\theta_{11} = \theta_{21} + \pi$. Similar to the analysis before, the coupled-mode equations are given by

$$\frac{\partial}{\partial t} \begin{bmatrix} A_1 \\ A_2 \end{bmatrix} = \begin{bmatrix} -if_1 - \gamma_{1,NR} - \gamma_{1,R} & -i\kappa \\ -i\kappa & -if_2 - \gamma_{2,NR} - \gamma_{2,R} \end{bmatrix} \begin{bmatrix} A_1 \\ A_2 \end{bmatrix} + \begin{bmatrix} -\sqrt{\gamma_{1,R}S_{1+}} \\ -i\sqrt{\gamma_{2,R}S_{1+}} \end{bmatrix} \quad (S22)$$

$$\begin{bmatrix} S_{1-} \\ S_{2-} \end{bmatrix} = \begin{bmatrix} 0 \\ S_{1+} \end{bmatrix} + \begin{bmatrix} -\sqrt{\gamma_{1,R}} & -i\sqrt{\gamma_{2,R}} \\ \sqrt{\gamma_{1,R}} & -i\sqrt{\gamma_{2,R}} \end{bmatrix} \begin{bmatrix} A_1 \\ A_2 \end{bmatrix} \quad (S23)$$

Under the perfect absorption condition, both Eq. (S24) and Eq. (S25) should be satisfied

$$\gamma_{2,R}\gamma_{1,NR} - \gamma_{1,R}\gamma_{2,NR} = 2\kappa\sqrt{\gamma_{1,R}\gamma_{2,R}} \quad (\text{S24})$$

$$\gamma_{1,R}\gamma_{2,R} - \gamma_{1,NR}\gamma_{2,NR} = \kappa^2 \quad (\text{S25})$$

Eq. (S24) and Eq. (S25) can be further re-expressed as

$$\frac{\gamma_{1,NR}}{\gamma_{1,R}} = 1 + \frac{\kappa}{\sqrt{\gamma_{1,R}\gamma_{2,R}}} \quad (\text{S26})$$

$$\frac{\gamma_{2,NR}}{\gamma_{2,R}} = 1 - \frac{\kappa}{\sqrt{\gamma_{1,R}\gamma_{2,R}}} \quad (\text{S27})$$

4. Numerical simulation

The absorption spectra and the eigenfrequencies of the two modes are calculated using the software COMSOL Multiphysics (5.3a). For each mode, the total decay rate γ_{tot} is equal to the calculated $\text{Im}(f_{\text{eigen}})$. The radiative decay rate γ_{R} is calculated using the same geometry parameters, except that Ge is supposed to be lossless in calculation. The non-radiative decay rate γ_{NR} is determined by $\gamma_{\text{NR}} = \gamma_{\text{tot}} - \gamma_{\text{R}}$. In the simulations, the Si and SiO2 are set to be lossless dielectric with the respective refractive index $n_{\text{Si}} = 3.46$ and $n_{\text{SiO}_2} = 1.45$. The optical constants of Ge are from [2].

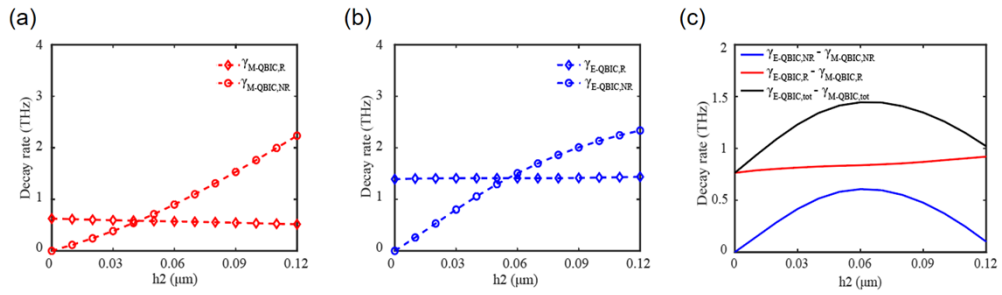


Fig. S2. **Dependence of decay rates on Ge thickness h_2 .** (a) Radiative and non-radiative decay rates of M-QBIC mode at different h_2 . (b) Radiative and non-radiative decay rates of E-QBIC mode at different h_2 . (c) Decay rates difference of the two modes at different h_2 .

The influence of h_2 on decay rates can be seen in Fig. S2. The non-radiative decay rates of both modes increase with h_2 due to the increase of intrinsic absorption of Ge, while their radiative decay rates hardly change with h_2 [Figs. S2(a), S2(b)]. The dependence of decay rates difference on h_2 are plotted in Fig. S2(c), where the total decay rates difference reaches maximum at $h_2 = 0.060 \mu\text{m}$. In the simulation, the following parameters are used: $h_1 = 0.330 \mu\text{m}$, $\theta = 9^\circ$, $a = 0.075 \mu\text{m}$, $b = 0.225 \mu\text{m}$, $P_y = 0.740 \mu\text{m}$, and $P_x = 0.620 \mu\text{m}$.

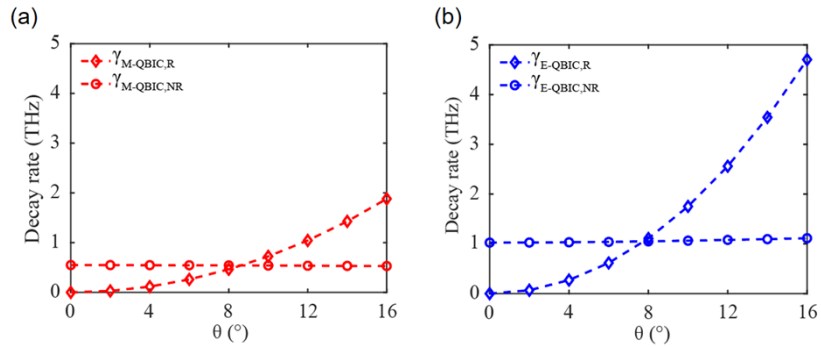


Fig. S3. **Dependence of decay rates on the orientation angle θ .** (a) Radiative and non-radiative decay rates of M-QBIC mode at different θ . (b) Radiative and non-radiative decay rates of M-QBIC mode at different θ .

The influence of θ on decay rates can be seen in Fig. S3. For M-QBIC and E-QBIC, the radiative decay rates increase with θ , while the non-radiative decay rates hardly change with θ . In the simulation, the following parameters are used: $h_1 = 0.330\mu\text{m}$, $h_2 = 0.040\mu\text{m}$, $a = 0.075\mu\text{m}$, $b = 0.225\mu\text{m}$, $P_y = 0.740\mu\text{m}$, $P_x = 0.620\mu\text{m}$.

Table S1. The values of P_x at different h_2 in Fig. 2(a) of the main text

$h_2(\mu\text{m})$	$P_x(\mu\text{m})$	$h_2(\mu\text{m})$	$P_x(\mu\text{m})$
0	0.733	0.038	0.713
0.010	0.726	0.040	0.713
0.015	0.723	0.045	0.712
0.020	0.721	0.050	0.712
0.025	0.718	0.060	0.713
0.030	0.716	0.070	0.716
0.035	0.714		

5. Field distributions of eigenmodes

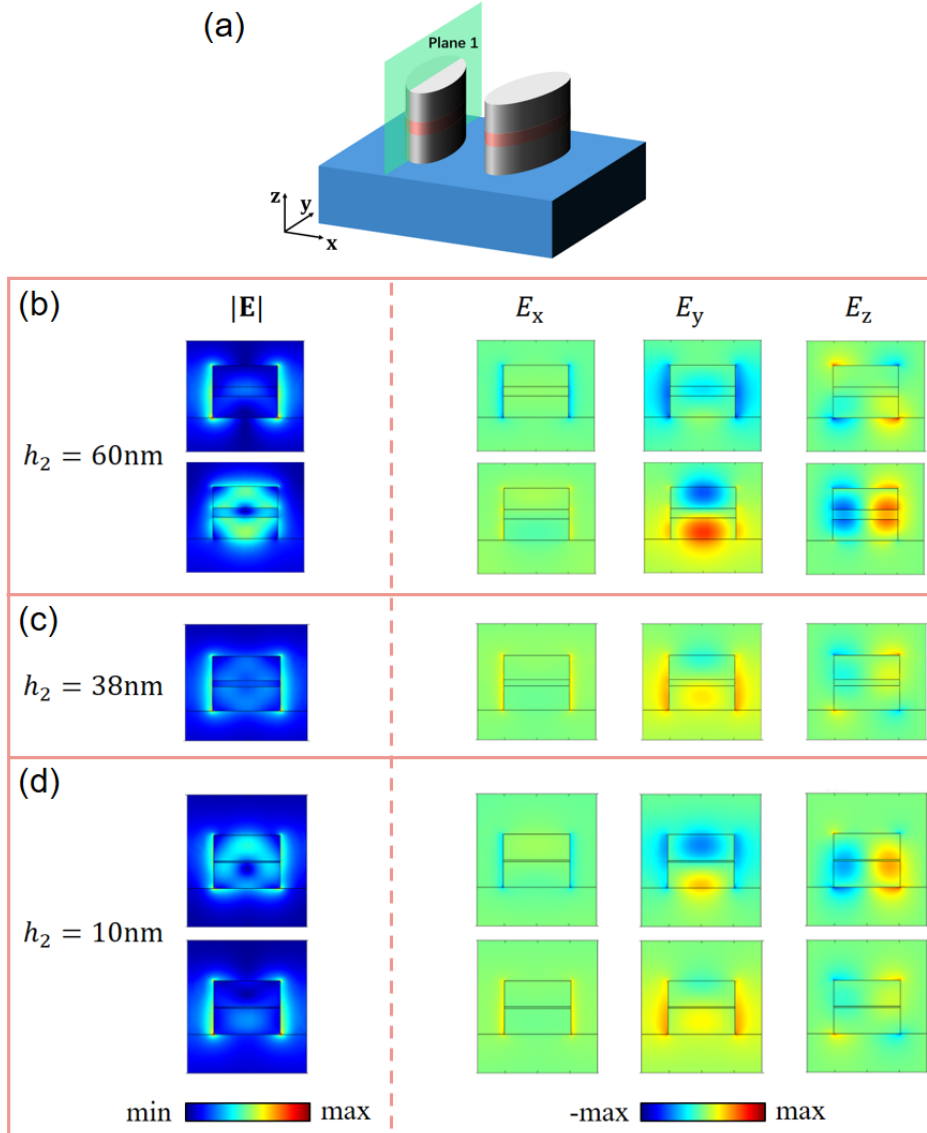


Fig. S4. **Eigenmode distributions in plane 1.** (a) Schematic of the metasurface. (b) - (d) Electric field distributions ($|\mathbf{E}|, E_x, E_y, E_z$) at different Ge thicknesses: (b) $h_2 = 60\text{nm}$, (c) $h_2 = 38\text{nm}$, and (d) $h_2 = 10\text{nm}$. The three thicknesses correspond to the three cases of Fig. 2(c) in the main text.

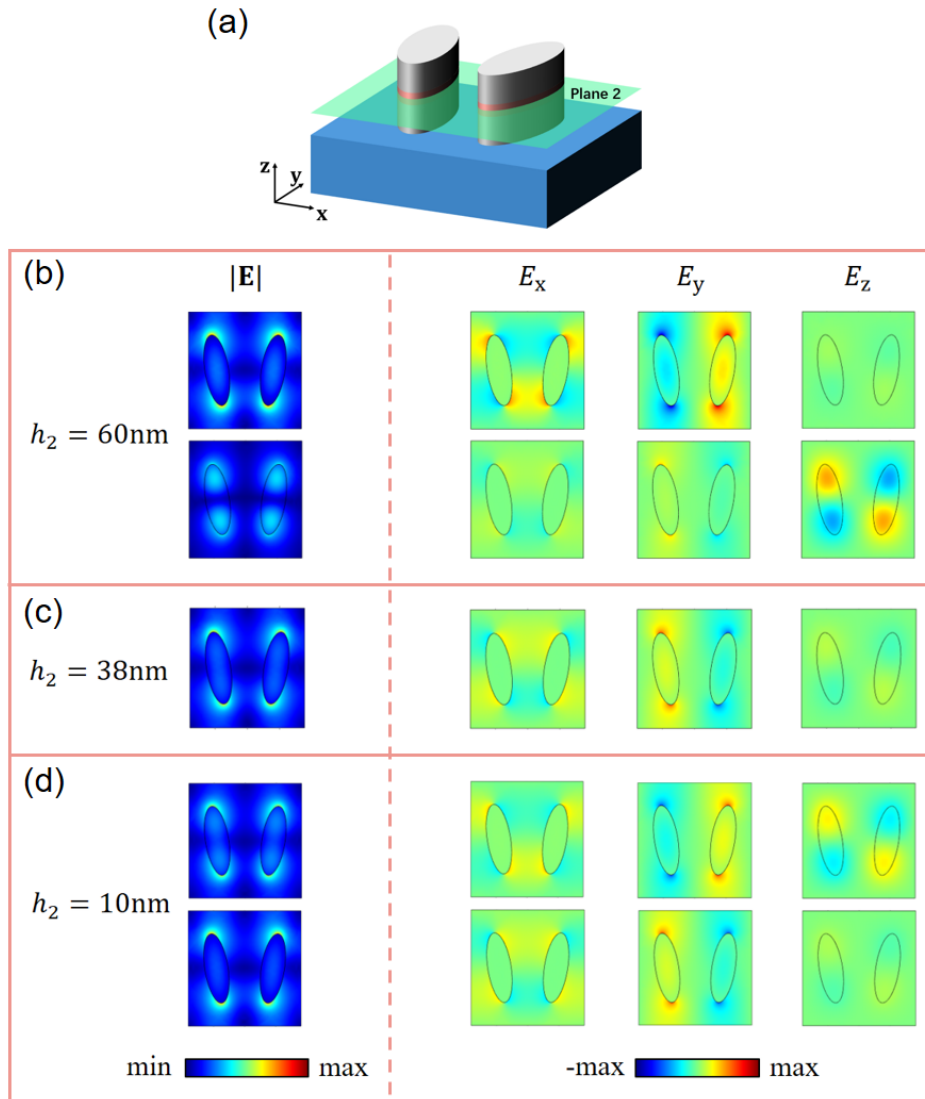


Fig. S5. **Eigenmode distributions in plane 2.** (a) Schematic of Plane 2. (b) - (d) Electric field distributions ($|\mathbf{E}|, E_x, E_y, E_z$) at different Ge thicknesses: (b) $h_2 = 60\text{nm}$, (c) $h_2 = 38\text{nm}$, and (d) $h_2 = 10\text{nm}$. The three thicknesses correspond to the three cases of Fig. 2(c) in the main text.

6. Sample fabrication and spectra measurement

To fabricate the sample, a 145-nm-thick Si film, a 40-nm-thick Ge film, and a 145 nm-thick Si film were sequentially deposited onto the SiO₂ substrate using magnetron sputtering (Denton DISCOVERY635). Thereafter, a 300-nm-thick negative resist (AR-N 7520) was spin coated and baked for 1 min at 90 ° C. Then a 50 nm-thick conductive protective coating (ARPC 5090.02) was spin coated, and the sample was exposed with EBL (VOYAGER, 50kV). After exposure, the sample was developed in AR 300-47 developer followed by rinsing in deionized water. Finally, the sample was etched using inductively coupled plasma-reactive ion etching (Oxford Plasmapro100 Cobra 180), and the residual resist is removed by AR 300-70.

The absorption A are characterized by measuring the reflection R and transmission T , and then using the equation $A=1-R-T$. The reflection and transmission spectra are measured by the setup shown in Fig. S6.

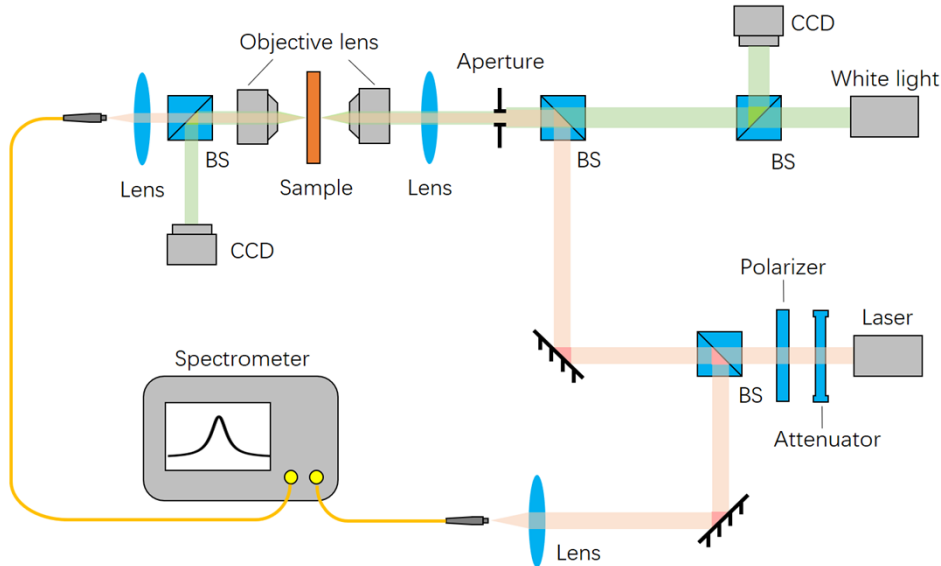


Fig. S6. **Sketch of the experimental setup.** BS stands for the beam splitter. The source for measurement is a super continuum laser (600nm – 1700nm), and the white light source is used to help to focus and image, which is turned off during spectra measurement.

Reference

1. W. Suh, Z. Wang, and S. Fan, "Temporal coupled-mode theory and the presence of non-orthogonal modes in lossless multimode cavities," *IEEE J. Quantum Electronics* **40**, 1511-1518 (2004).
2. E. D. Palik, "Handbook of optical constants of solids," (Academic Press, San Diego, 1998), Vol. III.